



MDA5 ISGylation is crucial for immune signaling to control viral replication and pathogenesis

Lucky Sarkar^a , GuanQun Liu^{a,1} , Dhiraj Acharya^a , Junji Zhu^a , Zuberwasim Sayyad^a , and Michaela U. Gack^{a,2}

Affiliations are included on p. 11.

Edited by Peter Palese, Icahn School of Medicine at Mount Sinai, New York, NY; received October 1, 2024; accepted March 6, 2025

The posttranslational modification (PTM) of innate immune sensor proteins by ubiquitin or ubiquitin-like proteins is crucial for regulating antiviral host responses. The cytoplasmic dsRNA receptor melanoma differentiation-associated protein 5 (MDA5) undergoes several PTMs including ISGylation within its first caspase activation and recruitment domain (CARD), which promotes MDA5 signaling. However, the relevance of MDA5 ISGylation for antiviral immunity in an infected organism has been elusive. Here, we generated knock-in mice (MDA5^{K23R/K43R}) in which the two major ISGylation sites, K23 and K43, in MDA5, were mutated. Primary cells derived from MDA5^{K23R/K43R} mice exhibited abrogated endogenous MDA5 ISGylation and an impaired ability of MDA5 to form oligomeric assemblies, leading to blunted cytokine responses to MDA5 RNA-agonist stimulation or infection with encephalomyocarditis virus (EMCV) or West Nile virus. Phenocopying MDA5^{-/-} mice, the MDA5^{K23R/K43R} mice infected with EMCV displayed increased myocardial injury and mortality, elevated viral titers, and an ablated induction of cytokines and chemokines compared to WT mice. Molecular studies identified human HERC5 (and its functional murine homolog HERC6) as the primary E3 ligases responsible for MDA5 ISGylation and activation. Taken together, these findings establish the importance of CARD ISGylation for MDA5-mediated RNA virus restriction, promoting potential avenues for immunomodulatory drug design for antiviral or anti-inflammatory applications.

antiviral innate immunity | MDA5 | interferon | ISGylation | virus infection

Innate immune surveillance serves as the body's first line of defense mechanism against a plethora of intruding pathogens whereby pathogen-associated molecular patterns (PAMPs) such as viral RNA and DNA are recognized (1–3). Upon sensing pathogenic “nonself” nucleic acids, germline-encoded pattern-recognition receptors (PRRs) expressed in innate immune (e.g., macrophages) and nonimmune (e.g., epithelial or fibroblast) cells confer an amplitude of host antiviral responses. These include 1) type I or III interferon (IFN)-mediated immunity, 2) the induction of proinflammatory cytokines, and 3) upregulation of IFN-stimulated genes (ISGs) in response to type I or III IFN receptor activation and JAK-STAT1/2 signaling. Ultimately, this complex innate immune program initiated by PRRs leads to the activation of adaptive immunity (typically mediated by T and B cells) (4).

Innate immunity in response to viral RNA sensing in the cytoplasm is orchestrated by several receptor proteins, primarily the RIG-I-like receptors (RLRs) retinoic acid-inducible gene-I (RIG-I) and MDA5 (5). These RNA helicases detect specific RNA species, such as 5'-triphosphate-containing RNA (RIG-I) or longer and more complex dsRNA structures (MDA5), after RNA virus infections. Besides RNA viruses, herpesviruses and adenoviruses also activate RLRs where either viral RNAs or certain mislocalized or modified host RNAs harboring signature immunostimulatory features (i.e., 5'-triphosphate moiety and dsRNA portions) are recognized (6, 7). This RNA sensing event then triggers a signaling cascade that is mediated by mitochondrial antiviral-signaling protein (MAVS) and the TBK1-IRF3/7 axis, promoting a transcriptional program comprising IFNs, antiviral effectors (typically the gene products of ISGs), and proinflammatory cytokine or chemokine molecules (5, 8). The antiviral program induced by RLRs ultimately suppresses the replication of diverse RNA viruses (such as flaviviruses, influenza viruses, and coronaviruses) and can also prompt tissue inflammation (9).

Protein posttranslational modifications (PTMs) modulate the physiological functions of cells by altering protein conformation, activity, stability, and/or localization (10). In particular, innate immune sensors are intricately regulated by a “PTM-code” that determines the timing and/or magnitude of PRR activation (5, 11). On the other hand, PTMs can also negatively regulate sensor activation, curbing excessive cytokine responses that

Significance

The work by many groups demonstrated the important role of ubiquitination in modulating the activity of innate immune sensors. In contrast, little is still known about the significance of ISGylation in immune receptor regulation. In this study, we generated knock-in mice in which the two major ISGylation sites of the RNA sensor MDA5 were mutated. Cells from these MDA5-ISGylation-defective mice showed impaired MDA5 oligomerization and antiviral signaling compared to WT mice. Virus-infected MDA5 knock-in mice displayed ablated antiviral responses, uncontrolled viral replication, and higher mortality. Our study identified HERC5 as the E3 ligase responsible for MDA5 ISGylation and activation. These data may offer opportunities for immune-based antiviral drug design or ways to alleviate inflammatory diseases associated with overzealous MDA5 activation.

Author contributions: L.S., G.L., D.A., J.Z., Z.S., and M.U.G. designed research; L.S., G.L., D.A., J.Z., and Z.S. performed research; L.S., G.L., D.A., J.Z., and Z.S. analyzed data; M.U.G. supervised the study; and L.S., G.L., and M.U.G. wrote the paper.

The authors declare no competing interest.

This article is a PNAS Direct Submission.

Copyright © 2025 the Author(s). Published by PNAS. This article is distributed under [Creative Commons Attribution-NonCommercial-NoDerivatives License 4.0 \(CC BY-NC-ND\)](https://creativecommons.org/licenses/by-nc-nd/4.0/).

¹Present address: Department of Microbiology and Immunology, McGill University, Montreal, Québec, QC H3A 2B4, Canada.

²To whom correspondence may be addressed. Email: gackm@ccf.org.

This article contains supporting information online at <https://www.pnas.org/lookup/suppl/doi:10.1073/pnas.2420190122/-/DCSupplemental>.

Published April 4, 2025.

can lead to deleterious outcomes such as autoimmune conditions. Serine/threonine phosphorylation and lysine ubiquitination are the most well-characterized PTMs regulating RLR activity (5). In unstimulated or uninfected cells, MDA5 and RIG-I are phosphorylated in their N-terminal caspase activation and recruitment domains (CARDs) and C-terminal domain (CTD) (12–15). CARD dephosphorylation by a phosphatase complex composed of protein phosphatase 1 alpha or gamma (PP1 α/γ) and the RIG-I/MDA5-targeting subunit PPP1R12C, allows for RLR transition from their signaling-restrained states to signal-transducing “active” forms (13, 16). Specifically, RNA virus infection releases PPP1R12C tethered to actin filaments, allowing its recruitment to RIG-I and MDA5 as part of a catalytically active PP1 complex to dephosphorylate the RLR CARDs. Similarly, the CTD of RLRs is dephosphorylated after RNA virus infection (12). Dephosphorylated RIG-I then undergoes TRIM25- and Riplet-mediated K63-linked polyubiquitination in its CARDs and CTD, respectively (17, 18). These polyubiquitination modifications promote and stabilize RIG-I oligomer formation and thereby induce its activation to initiate signaling via MAVS (5). MDA5 was shown to undergo K63-linked ubiquitination in its helicase domain catalyzed by the E3 ubiquitin ligase TRIM65, which facilitates MDA5 activation and downstream signaling (19). Whether the MDA5 CARDs undergo K63-linked ubiquitination in cells (vs. cell-free systems) has been controversial (5), prompting research investigations into activating PTMs in the MDA5 CARDs triggered by MDA5 dephosphorylation. Our recent study revealed that MDA5 dephosphorylation induces MDA5 CARD ISGylation (i.e., conjugation with the ubiquitin-like protein ISG15) at two major sites, K23 and K43 (20). MDA5 ISGylation drives antiviral IFN responses restricting a range of RNA viruses including encephalomyocarditis virus (EMCV), Zika virus, and severe acute respiratory syndrome coronavirus 2 (SARS-CoV-2) in human cells (20). Conversely, as a viral tactic evolved to escape ISGylation-dependent MDA5 signaling, the SARS-CoV-2 papain-like protease (PLpro) actively removes ISG15 from the MDA5 CARDs (20, 21). The physiological function of MDA5 ISGylation at the endogenous protein level and its *in vivo* relevance for controlling virus infection, however, have not yet been elucidated.

In this study, we generated MDA5^{K23R/K43R} knock-in mice and showed that the combined mutation of K23 and K43 ablated endogenous MDA5 ISGylation and oligomerization and thereby MDA5-mediated antiviral cytokine responses, leading to uncontrolled RNA virus-induced pathogenesis. Furthermore, we identified human HERC5 (or HERC6, the functional murine homolog) as the E3 ligase enzyme responsible for catalyzing MDA5 ISGylation, enabling MDA5 activation and antiviral signaling.

Results

Ablated MDA5 ISGylation and Oligomerization in Cells from MDA5^{K23R/K43R} Mice. Our previous work indicated that human MDA5 (hMDA5) undergoes ISGylation at K23 and K43 in the first CARD and that ISGylation promotes MDA5 signaling ability (20). As K23 and K43 are highly conserved in MDA5 across mammalian species including mice (*SI Appendix, Fig. S1A*), we sought to determine the physiological relevance of MDA5 CARD ISGylation at the endogenous protein level and for host antiviral defense *in vivo*. To this end, we generated MDA5 knock-in mice (termed MDA5^{K23R/K43R}) by introducing the K23R and K43R mutations into the native *Mda5/Ifib1* locus using CRISPR-Cas9 technology and a targeting repair vector containing the double mutant exon 1 to replace the WT exon 1 (Fig. 1 *A* and *B*, and

SI Appendix, Fig. S1B and *Materials and Methods*). In parallel, MDA5^{-/-} mice in which the exon 1 genomic region was deleted due to nonhomologous end joining (NHEJ) were generated as a matched control. All mouse lines were screened and validated using a three-set PCR genotyping strategy and by genomic DNA sequencing (Fig. 1 *B* and *SI Appendix, Fig. S1B* and *Materials and Methods*).

We next assessed the protein abundance of endogenous MDA5 in primary mouse dermal fibroblasts (MDFs) isolated from the three mouse lines both in unstimulated (basal) conditions and after exogenous IFN- α stimulation (Fig. 1 *C*). This showed comparable endogenous MDA5 protein expression in the cells from WT and MDA5^{K23R/K43R} mice, and further, confirmed the absence of MDA5 expression in the cells from MDA5^{-/-} mice. Notably, equal RIG-I and downstream ISG (i.e., IFIT2 and ISG15) protein expression was observed after IFN- α stimulation in the MDFs from all three mouse lines (Fig. 1 *C*), demonstrating intact IFN- α/β receptor (IFNAR) signaling. Next, we tested the ISGylation of endogenous MDA5 in MDFs isolated from MDA5^{K23R/K43R} or WT mice under basal (unstimulated) conditions or after stimulation with EMCV RNA, a specific agonist of MDA5 (5, 22) (Fig. 1 *D*). Of note, experimental conditions were chosen where ISG15 protein expression was comparable in both WT and knock-in mouse cells, allowing us to unambiguously compare the ISGylation of WT and mutant MDA5. Consistent with our previous study (20), we detected low-level basal ISGylation for endogenous MDA5 in WT cells. However, this basal ISGylation was absent in cells from MDA5^{K23R/K43R} mice. Furthermore, cells from WT mice showed robust endogenous MDA5 ISGylation after EMCV RNA stimulation. In contrast, EMCV RNA-stimulated cells from MDA5^{K23R/K43R} mice exhibited a near-abolished ISGylation of endogenous MDA5 (Fig. 1 *D*). Importantly, the levels of K63-linked polyubiquitination and SUMOylation of endogenous MDA5 (19, 23) in cells from MDA5^{K23R/K43R} and WT mice were comparable (Fig. 1 *E* and *F*), strengthening our previous data (20) that showed that the mutation of K23 and K43 specifically abrogates ISG15 conjugation but does not affect—directly or indirectly—MDA5 ubiquitination or SUMOylation.

Upon binding to dsRNA in the cytosol, hMDA5 is primed by CARD ISGylation facilitating its multimerization (20). Consistent with these previous findings on exogenous WT and K23R/K43R hMDA5, endogenous mMDA5 exhibited efficient oligomerization in EMCV RNA-stimulated MDFs from WT control mice; however, endogenous mMDA5 oligomerization was substantially impaired in cells derived from MDA5^{K23R/K43R} mice (Fig. 1 *G* and *H*, and *SI Appendix, Fig. S1 C and D*). Collectively, these findings show that endogenous MDA5 undergoes ISGylation at K23 and K43, which is important for its ability to oligomerize in response to RNA agonist stimulation.

MDA5 ISGylation Is Pivotal for Eliciting IFN and ISG Responses Against Picornavirus Infection in Fibroblasts. To elucidate the role of MDA5 ISGylation in downstream signal transduction, we assessed specific activating phosphorylation marks for IRF3 and TBK1 (both downstream of MDA5 and many other PRRs) as well as STAT1 (downstream of IFNAR) in MDF cells derived from WT and MDA5^{K23R/K43R} mice upon infection with EMCV. Cells from MDA5^{-/-} mice were included as a control. TBK1 and IRF3 phosphorylation was effectively elicited in cells from WT mice following EMCV infection. In contrast, cells derived from MDA5^{K23R/K43R} and MDA5^{-/-} mice showed impaired activating phosphorylations for TBK1 and IRF3 (Fig. 2 *A* and *SI Appendix, Fig. S2A*). In accord, EMCV-infected cells from WT mice, but not MDA5^{K23R/K43R} and MDA5^{-/-} mice, exhibited robust STAT1

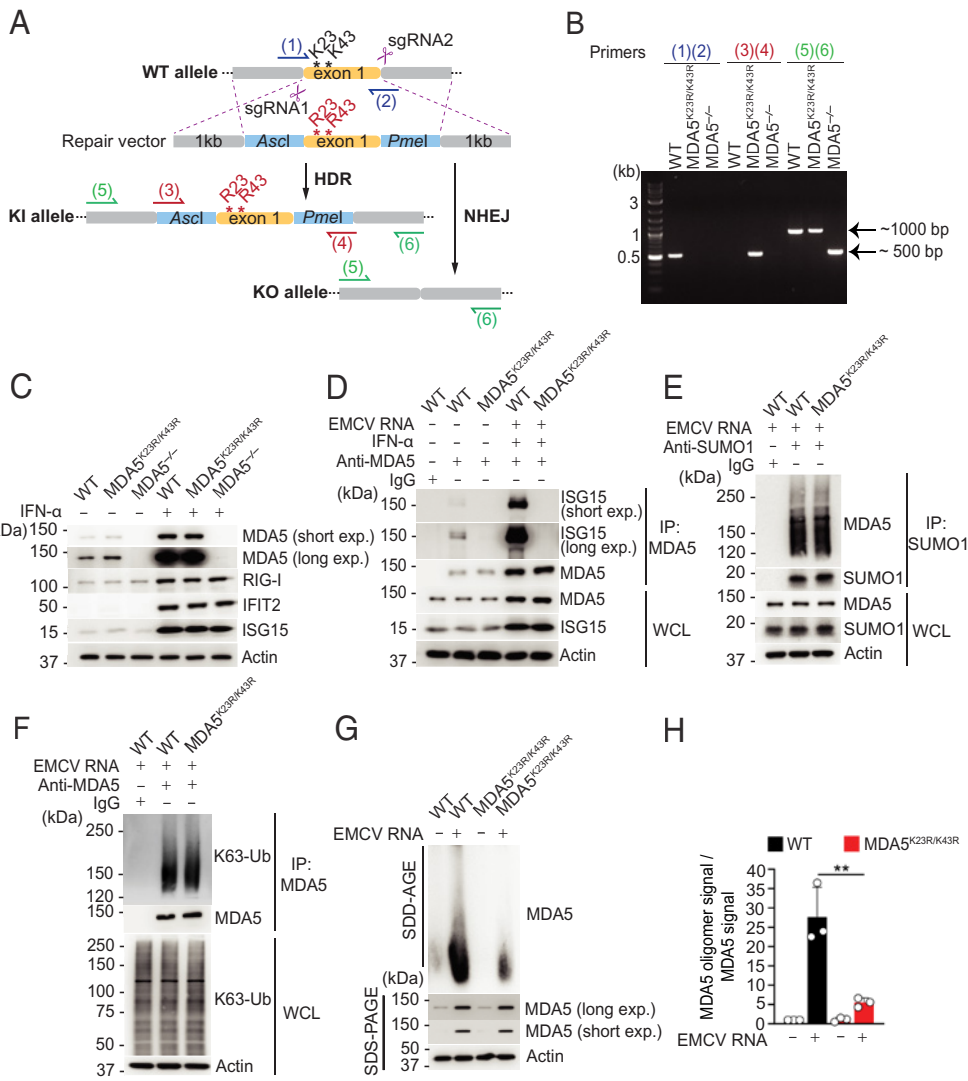


Fig. 1. Impaired MDA5 ISGylation and oligomerization in MDA5^{K23R/K43R} mouse cells. (A) Schematic of the CRISPR-Cas9 editing strategy for the generation of MDA5^{K23R/K43R} and control mice. See *Materials and Methods* and *SI Appendix, Fig. S1B* for details. The two conserved lysine residues (K23 and K43; codons AAA and AAA; black asterisks) were mutated to arginines (K23R/K43R; codons AGA and AGA; red asterisks). HDR, homology-directed repair. NHEJ, nonhomologous end-joining. sgRNA, single-guide RNA. (B) Schematic diagram of the validation strategy of the transgenic mouse lines by PCR genotyping. Genomic DNA isolated from ear tissue was amplified to detect the presence of *Mda5/Irfh1* mutant (K23R/K43R) exon1 locus using the indicated primers by agarose gel electrophoresis. The primer pair (1) and (2) generates a 523 bp-fragment in WT mice; the primer pair (3) and (4) generates a 537 bp-fragment in MDA5^{K23R/K43R} mice; and the primer pair (5) and (6) generates a 1,046 bp-fragment in WT mice, a 1,062 bp-fragment in MDA5^{K23R/K43R} mice, and a 565 bp-fragment in MDA5^{-/-} mice. (C) Analysis of the protein abundance of endogenous MDA5, RIG-I, and downstream ISGs (IFIT2 and ISG15) in the whole cell lysates (WCLs) of primary mouse dermal fibroblasts (MDFs) isolated from 6 to 8-wk-old WT, MDA5^{K23R/K43R}, and MDA5^{-/-} mice that were stimulated *ex vivo* with IFN- α (500 U/mL) for 24 h or that remained untreated (-), determined by immunoblot (IB) analysis. (D) Endogenous MDA5 ISGylation in MDFs from WT or MDA5^{K23R/K43R} mice that were either mock-treated or prestimulated for 8 h with IFN- α (1,000 U/mL) and then mock-stimulated or transfected with EMCV RNA (0.4 μ g/mL) for 16 h to stimulate MDA5 activation, determined by IP with anti-MDA5 (or an IgG isotype control) and IB with anti-ISG15. (E) Endogenous MDA5 SUMOylation in WT or MDA5^{K23R/K43R} mouse-derived MDFs transfected with EMCV RNA (0.4 μ g/mL) for 16 h, determined by IP with anti-SUMO1 (or an IgG isotype control) and IB with anti-MDA5. (F) K63-linked ubiquitination of endogenous MDA5 in MDFs from WT or MDA5^{K23R/K43R} mice that were transfected with EMCV RNA (0.4 μ g/mL) for 16 h, determined by IP with anti-MDA5 and IB with K63-polyubiquitin-linkage-specific antibody (K63-Ub). (G) Endogenous MDA5 oligomerization in WT and MDA5^{K23R/K43R} mouse-derived MDFs that were either mock-treated or transfected with EMCV RNA (0.4 μ g/mL) for 8 h, assessed by semidenaturing detergent agarose gel electrophoresis (SDD-AGE) and IB with anti-MDA5. The protein abundance of MDA5 in WT and MDA5^{K23R/K43R} MDFs was assessed by SDS-PAGE and IB with anti-MDA5 (with Actin as loading control). (H) Densitometric analysis of the MDA5 oligomer signal, normalized to the respective MDA5 protein abundance, for the experiment in (G). Values represent relative signal intensity normalized to values for unstimulated WT control cells, set to 1. Data are representative of at least two independent experiments [mean \pm SD of N = 3 biological replicates in (H)]. ***P* < 0.01 (two-tailed, unpaired Student's *t* test).

phosphorylation (Fig. 2B and *SI Appendix, Fig. S2B*). Importantly, MDFs from WT, MDA5^{K23R/K43R}, and MDA5^{-/-} mice showed comparable TBK1, IRF3, and STAT1 phosphorylations upon infection with Sendai virus (SeV, an RNA virus that is sensed by RIG-I), demonstrating the integrity of the RIG-I signaling pathway in the cells derived from MDA5^{K23R/K43R} and MDA5^{-/-} mice. Consistent with these results, the transcript expression of type I IFN (i.e., *Irfn1*), ISGs (i.e., *Mx1* and *Oas1b*), and proinflammatory cytokines and chemokines (i.e., *Tnf*, *Ccl5*, and *Cxcl10*) was efficiently elicited in MDFs from WT mice over a

time course of EMCV RNA stimulation. In comparison, antiviral and proinflammatory gene induction was impaired in EMCV RNA-transfected cells from MDA5^{K23R/K43R} and MDA5^{-/-} mice. Notably, MDA5^{-/-} mouse cells consistently showed a stronger diminishment of antiviral gene induction compared with the cells from MDA5^{K23R/K43R} mice (Fig. 2C–E and *SI Appendix, Fig. S2 C–E*). MDFs derived from WT, MDA5^{K23R/K43R}, and MDA5^{-/-} mice, however, responded equally well to rabies virus leader RNA [RABV_L; an RNA agonist activating RIG-I (24)] (Fig. 2C–E and *SI Appendix, Fig. S2 C–E*). In line with these

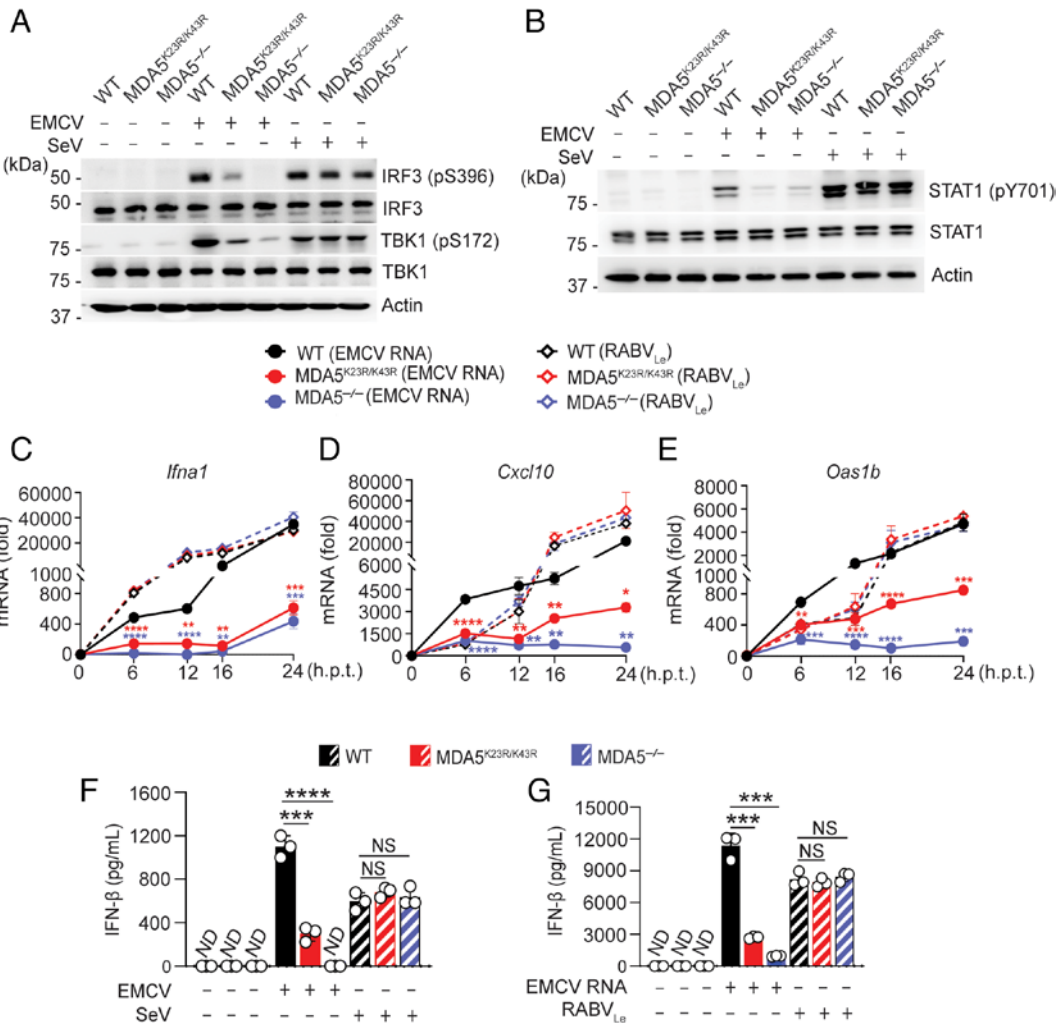


Fig. 2. Ablated MDA5 antiviral signaling in MDA5^{K23R/K43R} mouse-derived dermal fibroblasts. (A) IRF3 and TBK1 phosphorylation in WT, MDA5^{K23R/K43R}, and MDA5^{-/-} mouse-derived MDFs that were infected for 6 h with either EMCV (MOI 2) or SeV (250 hemagglutination units [HAU]/mL) or that remained uninfected (-), determined in the WCLs by IB with anti-pS396-IRF3, anti-IRF3, anti-pS172-TBK1, and anti-TBK1. (B) STAT1 phosphorylation in WT, MDA5^{K23R/K43R}, and MDA5^{-/-} mouse-derived MDFs that were infected for 12 h with either EMCV (MOI 2) or SeV (250 HAU/mL) or that remained uninfected (-), assessed in the WCLs by IB with anti-pY701-STAT1 and anti-STAT1. (C-E) *Ifna1*, *Cxcl10*, and *Oas1b* transcript abundance in WT, MDA5^{K23R/K43R}, and MDA5^{-/-} mouse-derived MDFs that were transfected with EMCV RNA (0.4 μg/mL) or RABV_{Le} (1 pmol/mL) for the indicated times, determined by RT-qPCR. (F and G) Secreted IFN-β protein in the supernatant of WT, MDA5^{K23R/K43R}, and MDA5^{-/-} mouse-derived MDFs that were either mock-treated (-) (F and G), infected for 12 h with EMCV (MOI 1) or SeV (20 HAU/mL) (F), or transfected for 12 h with EMCV RNA (0.4 μg/mL) or RABV_{Le} (1 pmol/mL) (G), determined by ELISA. Data are representative of at least two independent experiments (mean ± SD of N = 3 biological replicates in C-G). *P < 0.05, **P < 0.01, ***P < 0.001, ****P < 0.0001 (two-tailed, unpaired Student's *t* test). Red and blue asterisks in (C-E) indicate the statistical significance (*P*-values) for WT vs. MDA5^{K23R/K43R} and WT vs. MDA5^{-/-} (EMCV RNA-transfected) samples, respectively. h.p.t., hours posttransfection. ND, not detected. NS, statistically not significant.

data using RLR RNA ligands, authentic EMCV infection in cells from WT mice, but not in cells from MDA5^{K23R/K43R} and MDA5^{-/-} mice, effectively elicited antiviral gene responses, while SeV infection robustly stimulated an antiviral response in the cells from all three mouse lines (*SI Appendix*, Fig. S2 F-J). Consistent with our data on antiviral gene induction, we observed strongly diminished and ablated IFN-β protein secretion in MDFs derived from MDA5^{K23R/K43R} and MDA5^{-/-} mice, respectively (compared to cells from WT mice) after MDA5, but not RIG-I, stimulation (Fig. 2 F and G). These results indicate that ISGylation of endogenous MDA5 is required for its functional ability to instigate an antiviral cellular defense program.

ISG15 Conjugation of the MDA5 CARDS Is Required for Innate Signaling in Immune Cells. We next sought to determine the role of CARD ISGylation in MDA5 signaling in immune cells, in particular primary bone marrow-derived macrophages (BMDMs). Similar to our results obtained from MDFs, EMCV-infected BMDMs from MDA5^{K23R/K43R} and MDA5^{-/-} mice exhibited

strongly diminished phosphorylation of IRF3, TBK1, and STAT1 compared to BMDMs from WT mice (Fig. 3A and *SI Appendix*, Fig. S3 A and B). In accord, cytokine and chemokine gene expression upon EMCV infection or EMCV RNA transfection was impaired in MDA5^{K23R/K43R} cells compared to WT control cells (Fig. 3 B-D and *SI Appendix*, Fig. S3 C and D). In stark contrast, the signaling molecule activation and antiviral gene responses of SeV-infected or RABV_{Le}-transfected MDA5^{K23R/K43R} mouse-derived BMDMs were comparable to those in cells from WT mice (Fig. 3 B-D and *SI Appendix*, Fig. S3 C and D). These results show that immune cells derived from MDA5^{K23R/K43R} mice exhibit abrogated MDA5 antiviral signaling.

MDA5 ISGylation Is Important for Eliciting an Antiviral Transcriptional Program Against Coronaviruses and Flaviviruses. In addition to detecting picornavirus infections, MDA5 is a major receptor for sensing coronaviruses and flaviviruses (5). As such, we investigated the requirement of MDA5 ISGylation at K23 and K43 for initiating an innate transcriptional program

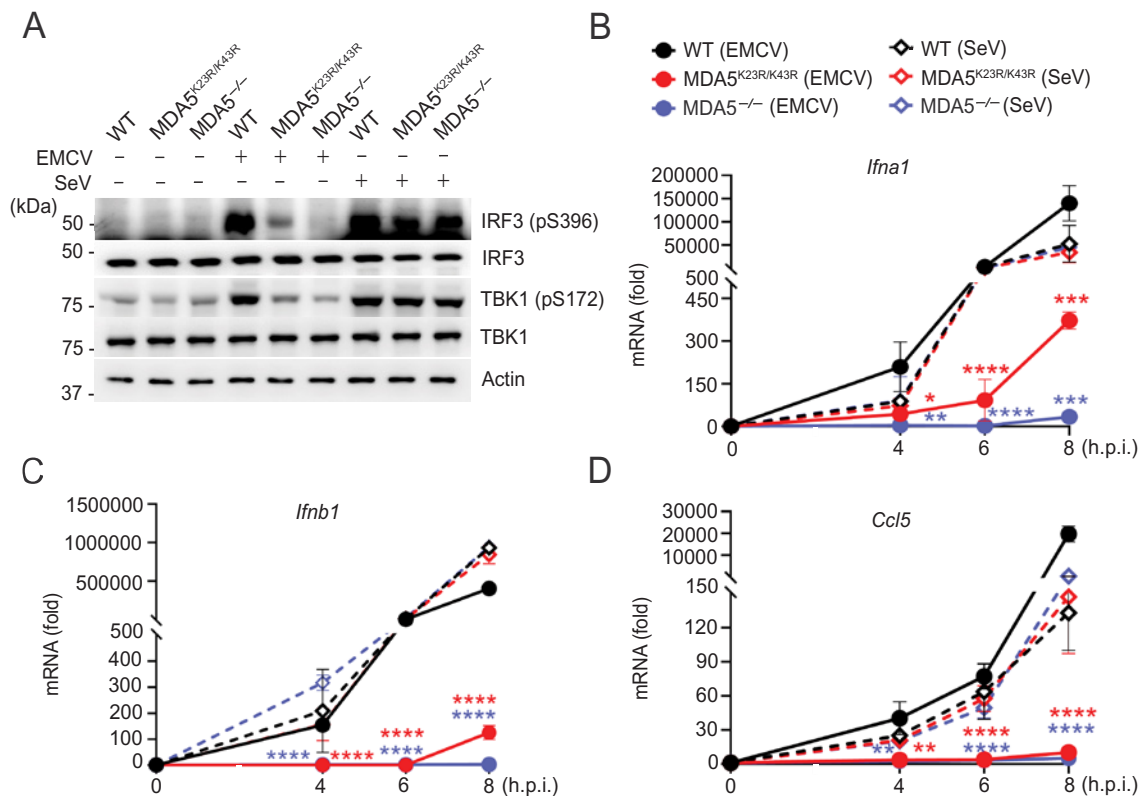


Fig. 3. Innate immune signaling to EMCV, but not SeV, infection is impaired in MDA5^{K23R/K43R} mouse-derived immune cells. (A) Phosphorylation of endogenous IRF3 and TBK1 in WT, MDA5^{K23R/K43R}, and MDA5^{-/-} mouse-derived BMDMs that were infected for 6 h with either EMCV (MOI 5) or SeV (200 HAU/mL), assessed in the WCLs by IB with anti-pS396-IRF3 and anti-pS172-TBK1. WCLs were further immunoblotted with anti-IRF3, anti-TBK1, and anti-Actin (loading control). (B–D) *Ifna1*, *Ifnb1*, and *Ccl5* transcripts in WT, MDA5^{K23R/K43R}, and MDA5^{-/-} mouse-derived BMDMs that were infected with either EMCV (MOI 1) or SeV (20 HAU/mL) for the indicated times. Data are representative of at least two independent experiments (mean \pm SD of N = 3 biological replicates in B–D). * P < 0.05, ** P < 0.01, *** P < 0.001, and **** P < 0.0001 (two-tailed, unpaired Student's t test). Red and blue asterisks in (B–D) indicate the statistical significance (P -values) for WT vs. MDA5^{K23R/K43R} and WT vs. MDA5^{-/-} (EMCV infected) samples, respectively. h.p.i., hours postinfection.

to SARS-CoV-2 (coronavirus) and West Nile virus (WNV, a flavivirus). Of note, we used SARS-CoV-2 RNA [which activates primarily MDA5 (20)], instead of authentic SARS-CoV-2 infection, because 1) ancestral SARS-CoV-2 is unable to efficiently infect primary mouse fibroblasts due to the absence of human ACE2 (the SARS-CoV-2 entry receptor) expression, and 2) the virus has effective mechanisms to dampen MDA5 signaling (20, 25). Transfection of SARS-CoV-2 RNA into MDFs derived from MDA5^{K23R/K43R} or MDA5^{-/-} mice induced little or no antiviral and proinflammatory gene expression as compared to that induced in WT cells (Fig. 4A). Moreover, MDA5^{K23R/K43R} or MDA5^{-/-} mouse-derived MDFs exhibited blunted antiviral transcriptional responses following authentic WNV infection as compared to control cells (Fig. 4B). Of note, in these experiments, we measured antiviral gene induction specifically at a late time (i.e., 60 h) in WNV infection where MDA5 was shown to play a major role in flaviviral RNA detection, whereas RIG-I senses WNV early in infection (26). In contrast, IFN/ISG transcriptional induction upon infection with influenza A virus (IAV), which is sensed by RIG-I (27, 28), was comparable in MDFs from WT, MDA5^{K23R/K43R}, and MDA5^{-/-} mice (Fig. 4C). Together with our data on EMCV, these findings strengthen the importance of CARD ISGylation for MDA5's ability to elicit an innate immune program against RNA viruses from at least three different families (i.e., *Picornaviridae*, *Coronaviridae*, and *Flaviviridae*).

HERC5/HERC6 Catalyzes MDA5 ISGylation, Promoting MDA5 Oligomerization and Immune Signal Transduction. To identify the E3 ligase(s) responsible for MDA5 CARD ISGylation, we

adopted a candidate approach in which we silenced specific enzymes known to have E3 ligase activity for ISG15 [i.e., HERC5 (29), HHARI or ARIH1 (Ariadne RBR E3 ubiquitin protein ligase 1 (30)), and TRIM25 (also named estrogen finger protein (EFP) (31)] and tested the effect of silencing on endogenous hMDA5 ISGylation. Knockdown of TRIM65, which mediates the K63-linked ubiquitination of MDA5's helicase domain (19) and is not known to confer ISG15 E3 ligase activity, served as a control in this experiment. Depletion of endogenous HERC5 ablated MDA5 ISGylation in primary normal human lung fibroblasts (NHLF) as compared to transfection of nontargeting control siRNA (si.C), whereas knockdown of the other E3 ligases had no diminishing effect on MDA5 ISGylation (Fig. 5A). Depletion of endogenous HERC6 [the functional substitute of HERC5 in mice (32, 33)] in primary MDFs near-abolished MDA5 ISGylation induced by EMCV RNA stimulation, to a similar extent as did E1 (UBE1L) or E2 (UBCH8) silencing (Fig. 5B). In contrast, depletion of endogenous TRIM65 in MDFs did not affect MDA5 ISGylation, ruling out that TRIM65—either directly or indirectly (for example, via a possible crosstalk between MDA5 K63-linked ubiquitination and ISGylation)—influences MDA5 ISGylation (Fig. 5B). In line with these findings, HERC6 knockdown in EMCV RNA-stimulated WT MDFs noticeably diminished MDA5 oligomerization. By contrast, HERC6 silencing in cells from MDA5^{K23R/K43R} mice, which showed impaired MDA5 oligomerization (as compared to cells from WT mice), did not further reduce MDA5 oligomerization (Fig. 5C and D).

Knockdown of HERC5, but not ARIH1, in primary NHLFs markedly reduced the levels of ISG, cytokine, and chemokine

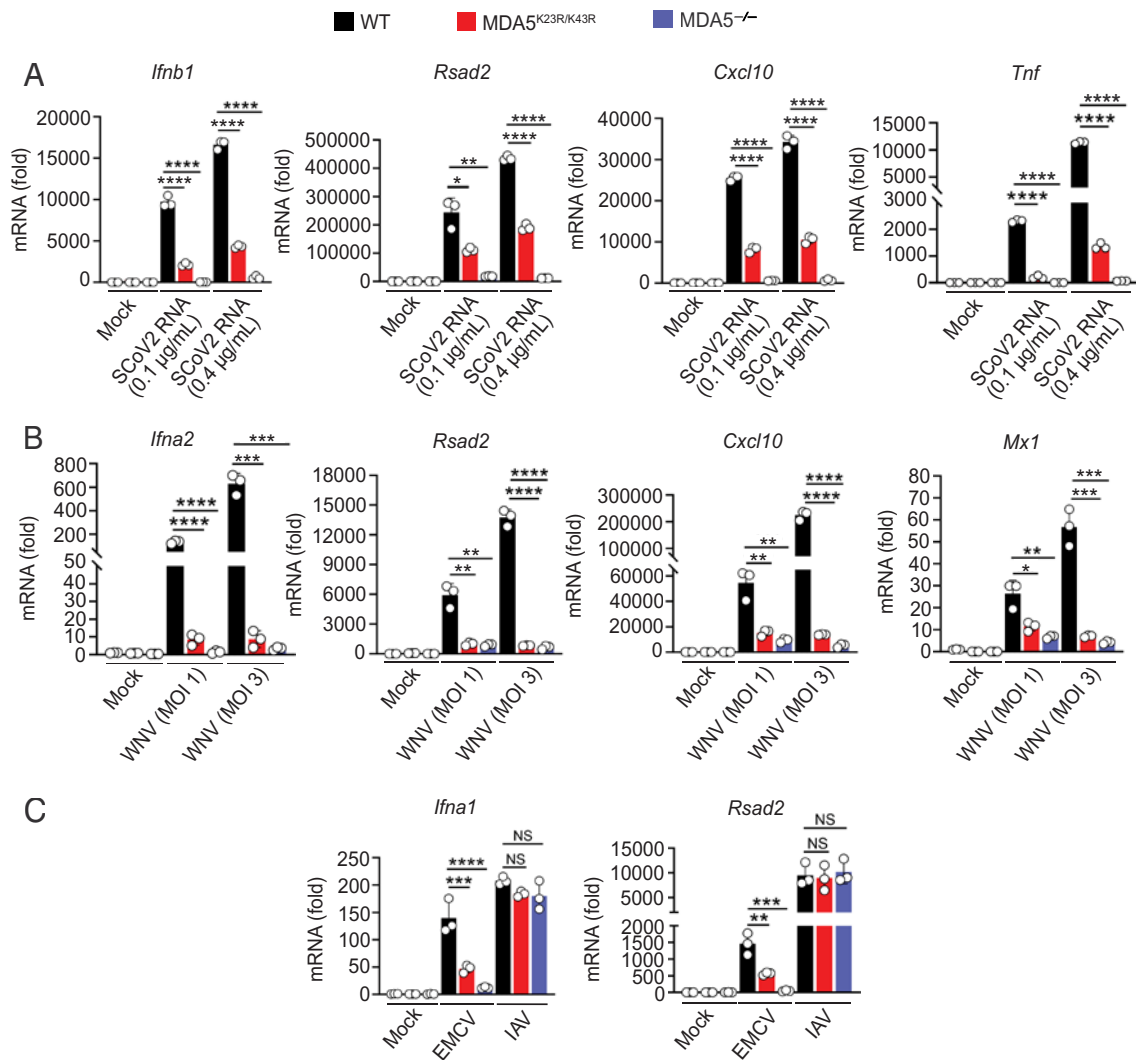


Fig. 4. MDA5^{K23R/K43R} mouse-derived cells are deficient in mounting an innate immune response to coronavirus or flavivirus challenge. (A) RT-qPCR analysis of the indicated antiviral or proinflammatory gene transcripts in WT, MDA5^{K23R/K43R}, and MDA5^{-/-} mouse-derived MDFs at 16 h posttransfection with SARS-CoV-2 RNA (0.1 or 0.4 μg/mL). Mock-treated cells served as control. (B) RT-qPCR analysis of the indicated genes in WT, MDA5^{K23R/K43R}, and MDA5^{-/-} mouse-derived MDFs that were either mock-treated or infected for 60 h with WNV (MOI 1 or 3). (C) RT-qPCR analysis of the indicated antiviral gene transcripts in WT, MDA5^{K23R/K43R}, and MDA5^{-/-} mouse-derived MDFs that were either mock-treated or infected for 8 h with either EMCV or IAV (each MOI 1). Data are representative of at least two independent experiments (mean ± SD of N = 3 biological replicates). *P < 0.05, **P < 0.01, ***P < 0.001, and ****P < 0.0001 (two-tailed, unpaired Student's *t* test). SCoV2, SARS-CoV-2. NS, statistically not significant.

transcripts upon EMCV RNA stimulation (Fig. 5E and *SI Appendix, Fig. S4A*). Similarly, the knockdown of endogenous HERC6 in WT MDFs abrogated EMCV RNA-induced antiviral gene expression as compared to si.C transfection (*SI Appendix, Fig. S4B*). The diminishing effect of HERC5 or HERC6 silencing on MDA5 signaling was observed with several different siRNAs having unique targeting sequences, ruling out potential off-target effects (*SI Appendix, Fig. S4 C and D*). Notably, HERC5 or HERC6 knockdown did however not ablate antiviral gene expression induced by RABV_{Lc} transfection (*SI Appendix, Fig. S5 A and B*). Collectively, these results establish that HERC5 (human) and HERC6 (mouse) are the major E3 ligases that mediate MDA5 ISGylation, ultimately promoting MDA5 oligomerization and antiviral signaling.

MDA5^{K23R/K43R} Mice are Impaired in Eliciting Effective Innate Immune Responses and in Restricting Virus Infection. To evaluate the *in vivo* relevance of ISGylation-dependent MDA5 activation in antiviral immunity, we infected WT and MDA5^{K23R/K43R} mice intraperitoneally with EMCV and monitored morbidity

and survival, innate immune responses, and viral titers (Fig. 6A). MDA5^{-/-} mice were included in these experiments for comparison. MDA5^{K23R/K43R} and MDA5^{-/-} mice infected with EMCV exhibited more severe clinical disease signs and accelerated lethality compared to infected WT mice (Fig. 6B and *SI Appendix, Methods, and Fig. S6A*). Analysis of EMCV replication revealed that MDA5^{K23R/K43R} and MDA5^{-/-} mice had significantly higher viral titers in cardiac and brain tissues as compared to WT mice (Fig. 6C and D), indicating enhanced viral replication due to ablated MDA5 activity in the MDA5^{K23R/K43R} and MDA5^{-/-} mice. Furthermore, effective IFN-β production was triggered in the blood of infected WT mice. In contrast, IFN-β protein was undetectable in the blood of infected MDA5^{K23R/K43R} and MDA5^{-/-} mice (Fig. 6E). In line with these results, RT-qPCR analysis detected higher viral RNA amounts and strongly reduced cytokine/chemokine transcript levels in the blood (Fig. 6F) and heart (Fig. 6G) of infected MDA5^{K23R/K43R} mice compared with infected WT control mice. Of note, the impaired antiviral transcriptional program observed for MDA5^{K23R/K43R} mice was comparable to that of infected MDA5^{-/-} mice, which also showed

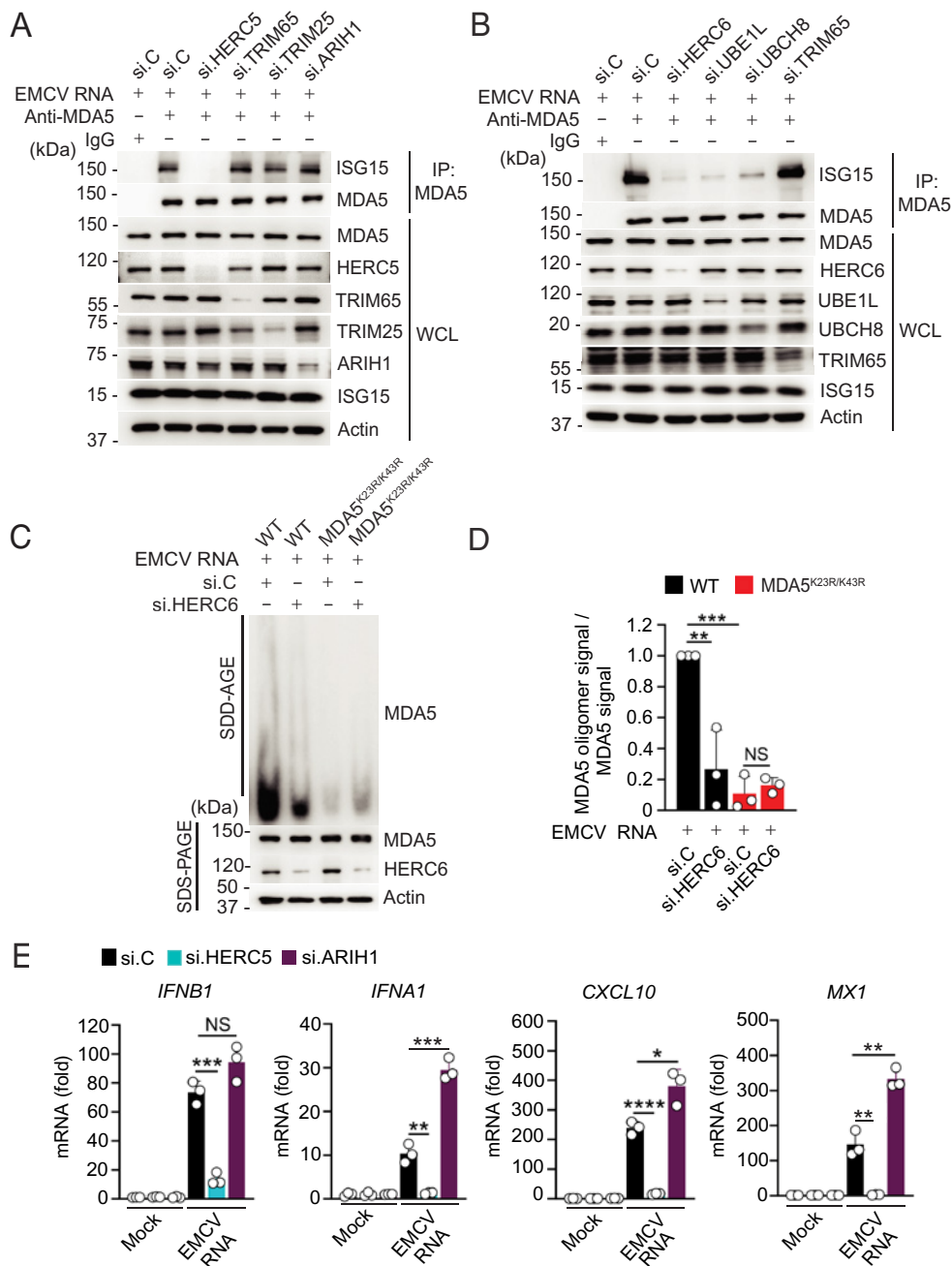


Fig. 5. HERC5/HERC6 catalyzes MDA5 ISGylation promoting MDA5 oligomerization and immune signaling. (A) ISGylation of endogenous MDA5 in primary NHLF cells that were transfected for 48 h with the indicated siRNAs and then transfected with EMCV RNA (0.4 $\mu\text{g}/\text{mL}$) for 16 h, determined by IP with anti-MDA5 (or an IgG isotype control) and IB with anti-ISG15. Knockdown of the individual genes was confirmed in the WCLs by IB with the indicated antibodies. (B) Endogenous MDA5 ISGylation in WT mouse-derived MDFs that were transfected for 48 h with the indicated siRNAs and then transfected with EMCV RNA (0.4 $\mu\text{g}/\text{mL}$) for 16 h, assessed as in (A). Knockdown of the individual genes was confirmed in the WCLs by IB with the indicated antibodies. (C) Endogenous MDA5 oligomerization in WT and MDA5^{K23R/K43R} mouse-derived MDFs that were transfected for 48 h with the indicated siRNAs and then transfected with EMCV RNA (0.4 $\mu\text{g}/\text{mL}$) for 16 h, assessed by SDD-AGE and IB with anti-MDA5. Input amounts for MDA5, as well as knockdown of endogenous HERC6, were confirmed by SDS-PAGE and IB with anti-MDA5 or anti-HERC6. (D) Densitometric analysis of the MDA5 oligomer signal, normalized to the respective MDA5 protein abundance, from the experiment in (C). Values represent relative signal intensity normalized to values for si.C-transfected WT cells, set to 1. (E) *IFNB1*, *IFNA1*, *CXCL10*, and *MX1* gene transcripts in primary NHLF cells that were transfected with the indicated siRNAs and then either Mock-treated or stimulated with EMCV RNA as in (A), determined by RT-qPCR. Data are representative of at least two (A, B, and E) or three (C and D) independent experiments [mean \pm SD of N = 3 biological replicates in (D and E)]. * $P < 0.05$, ** $P < 0.01$, *** $P < 0.001$, and **** $P < 0.0001$ (two-tailed, unpaired Student's *t* test). si.C, nontargeting control siRNA. NS, statistically not significant.

blunted cytokine/chemokine induction as expected (Fig. 6 *F* and *G*). Cumulatively, these results indicate that CARD ISGylation is a key activation mechanism for MDA5 to control RNA virus infection and viral pathogenesis in vivo.

MDA5 CARD ISGylation Is Cardioprotective During In Vivo EMCV Infection. To elucidate the impact of impaired MDA5 CARD ISGylation on EMCV-induced pathology, we performed

histological analysis of cardiac tissues from WT, MDA5^{K23R/K43R}, and MDA5^{-/-} mice. This revealed that EMCV-infected MDA5^{K23R/K43R} and MDA5^{-/-} mice exhibited markedly increased spacing between cardiac myofibers, indicative of edema caused by EMCV-induced cardiac damage (34), as compared to infected WT control mice (Fig. 7 *A* and *B*). In accord, the levels of cardiac troponin I (cTnI), a commonly used marker of myocardial injury, were significantly elevated in the plasma of EMCV-infected MDA5^{K23R/K43R}

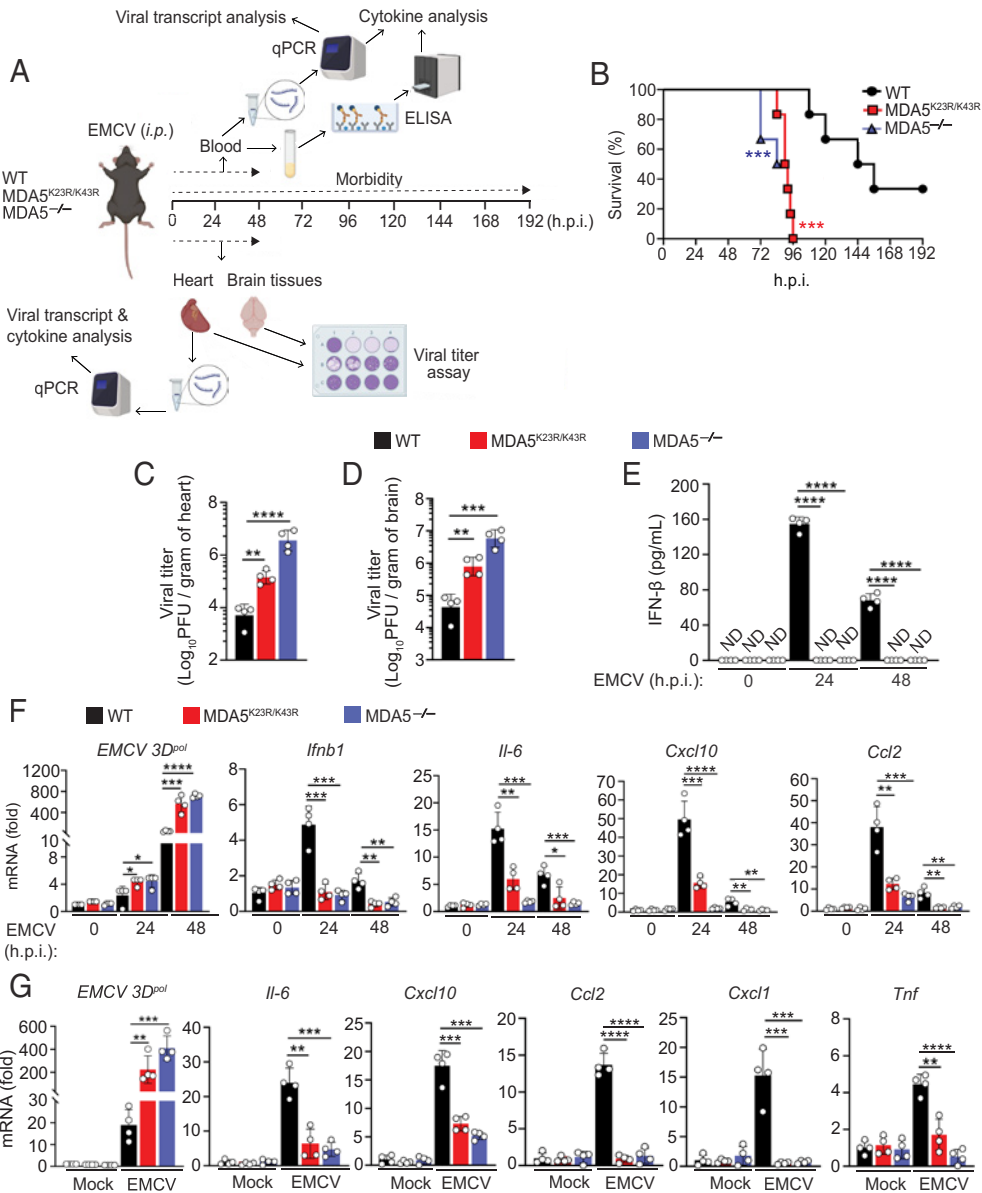


Fig. 6. ISGylation-defective MDA5^{K23R/K43R} mice exhibit ablated innate immune responses and are impaired in controlling EMCV infection. (A) Overview of the mouse infection studies with EMCV to measure morbidity and survival, viral replication, and cytokine responses. (B) WT, MDA5^{K23R/K43R}, and MDA5^{-/-} mice (6 to 8-wk-old) were infected via intraperitoneal (i.p.) inoculation with EMCV (25 PFU). Kaplan-Meier survival curves of EMCV-infected WT, MDA5^{K23R/K43R}, and MDA5^{-/-} mice (N = 6 per genotype). (C–G) WT, MDA5^{K23R/K43R}, and MDA5^{-/-} mice (6 to 8-wk-old) were infected via i.p. inoculation with EMCV (10³ PFU). Viral titers in the heart (C) and brain (D) were determined by plaque assay at 48 h.p.i., and (E) IFN-β protein in the blood was analyzed by ELISA at 24 and 48 h.p.i. Furthermore, EMCV 3D^{pol} as well as host antiviral or proinflammatory gene transcripts were measured in blood at 24 and 48 h.p.i. (F) and in heart tissue at 48 h.p.i. (G). Data are representative of at least two independent experiments [mean ± SD of N = 6 (B) or N = 4 (C–G) biological replicates]. *P < 0.05, **P < 0.01, ***P < 0.001, ****P < 0.0001. Mantel-Cox test (B) or two-tailed, unpaired Student's *t* test (C–G). h.p.i., hours postinfection. ND, not detected. Parts of Fig. 6A were created using Biorender.com.

and MDA5^{-/-} mice compared to infected WT mice (Fig. 7C). Collectively, these data indicate that ISGylation-dependent MDA5 activation is important for alleviating EMCV-induced cardiac pathology.

Discussion

Fine-tuning the signaling activity of the innate RNA sensor MDA5 has been shown to require several PTMs including phosphorylation, ubiquitination, SUMOylation, and lately, ISGylation (5). While the molecular discoveries on PTM-mediated MDA5 regulation have greatly advanced our understanding of MDA5 activation, the physiological relevance of several of these PTM marks, particularly in an organism, has been elusive. In the

present study, we generated MDA5^{K23R/K43R} mice with mutation of the two key ISGylation sites in MDA5 and investigated the direct contribution of ISGylation for MDA5-dependent antiviral innate immunity. We showed that, like human MDA5, endogenous mouse MDA5 undergoes robust ISGylation, and further, that this modification is crucial for MDA5's ability to form higher-order oligomeric assemblies and to induce antiviral IFN responses. Notably, this important role of MDA5 CARD ISGylation was observed for various MDA5 stimuli including MDA5-specific RNA ligands (i.e., EMCV RNA and SARS-CoV-2 RNA) and viruses from different families (i.e., *Picornaviridae* (EMCV) and *Flaviviridae* (WNV), both known to be detected by MDA5). Furthermore, similar to MDA5^{-/-} mice, MDA5^{K23R/K43R} mice were highly susceptible to EMCV

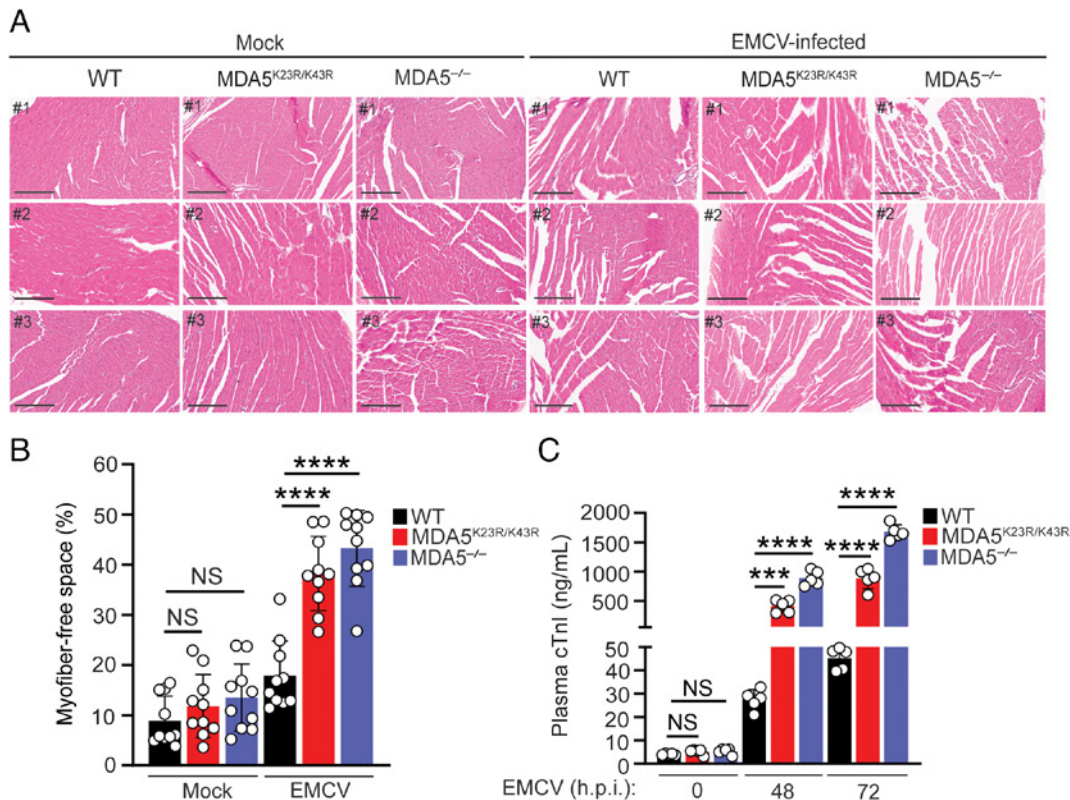


Fig. 7. MDA5^{K23R/K43R} mice exhibit severe myocardial injury after EMCV infection. (A) Representative images of hematoxylin and eosin (H&E)-stained heart tissue sections from WT, MDA5^{K23R/K43R}, and MDA5^{-/-} mice that were either mock-treated or infected via *i.p.* with 10³ PFU of EMCV for 72 h. #1–#3 indicate individual mice. Scale bar, 200 μ m. (B) Quantification of extracellular space between myofibers in the heart of WT, MDA5^{K23R/K43R}, and MDA5^{-/-} mice from the experiment in (A). (C) cTnI protein levels in plasma from WT, MDA5^{K23R/K43R}, and MDA5^{-/-} mice that were EMCV-infected as in (A), assessed by ELISA at the indicated times. Data in (B and C) represent mean \pm SD of N = 10 image fields (B) (see Methods for details on quantitative image analysis) or of N = 5 mice (C). ****P* < 0.001, *****P* < 0.0001. Two-tailed, unpaired Student's *t* test (B and C). h.p.i., hours postinfection. NS, statistically not significant.

infection and displayed heightened pathology and lethality owing to diminished antiviral IFN/cytokine and chemokine responses. Our data thus establish ISGylation as a physiologically important PTM governing MDA5 activation and its downstream antiviral signaling.

Our work also identified the E3 ligases catalyzing the CARD ISGylation marks of MDA5. Through a targeted siRNA-based miniscreen, we found that HERC5 and its functional murine homolog, HERC6, represent the key E3 ligases responsible for MDA5 ISGylation, prompting MDA5 downstream antiviral signaling. Interestingly, ISGylation has recently been shown to play important roles in the activation of the cGAS-mediated innate DNA sensing pathway (35–38). HERC5 and mouse HERC6 were also identified to be the critical E3 enzymes involved in the ISGylation of the DNA sensor cGAS and its signaling adaptor STING, promoting HSV-1 restriction (37, 38). These findings highlight HERC5/HERC6-mediated ISGylation as an essential regulatory arm of PRR-induced antiviral innate immunity against both RNA viruses and DNA viruses. While we have not tested directly the *in vivo* role of HERC6 in antiviral defense against MDA5-sensed viruses, a previous study showed that compared to WT mice, HERC6^{-/-} mice, despite exhibiting ablated global ISGylation, mounted comparable IFN and proinflammatory cytokine responses to infections with SeV and vesicular stomatitis virus, both known to be primarily sensed by RIG-I. This is consistent with our and others' observation that ISGylation positively regulates MDA5 signaling but has minimal or even opposing effects on RIG-I activation (20, 39, 40). Future studies are necessary to comprehensively assess the antiviral responses to MDA5- or RIG-I-sensed viruses in HERC6^{-/-} mice.

Our data strengthened the concept that HERC5/HERC6-mediated ISGylation of the N-terminal CARDS is important for efficient MDA5 oligomerization. Our observation that MDA5^{K23R/K43R} cells showed some residual MDA5 oligomerization and antiviral cytokine/ISG responses however indicates the involvement of other mechanisms in regulating MDA5 activation. In particular, the K63-linked polyubiquitination of MDA5 in the helicase domain by TRIM65 has been shown to facilitate MDA5 oligomerization and its downstream antiviral signaling (19). Indeed, silencing of endogenous TRIM65 in WT cells led to a reduction in MDA5 oligomerization to the levels of oligomerization observed for MDA5^{K23R/K43R} knock-in cells, whereas TRIM65 depletion in the MDA5^{K23R/K43R} knock-in background near-abolished MDA5 oligomerization (*SI Appendix, Fig. S6B*). These data suggest that MDA5 CARD ISGylation and helicase K63-linked ubiquitination play synergistic roles in facilitating MDA5 oligomerization, leading to optimal MDA5 activation. Given the role of the helicase domain in the initial binding to dsRNA ligands, it is tempting to speculate that the TRIM65-mediated ubiquitination of MDA5 occurs first and primes oligomerization, while CARD ISGylation amplifies the magnitude of MDA5 oligomeric assembly and downstream signal transduction. However, additional studies are needed to define the temporal aspects and respective roles of the CARD and helicase PTM-events in the MDA5 oligomerization process, and their relationships to other cofactors needed for MDA5 higher-order assembly formation.

A previous study reported that MDA5 undergoes SUMOylation in the CARDS at K43 (23). However, we observed similar levels of MDA5 SUMOylation (and also K63-linked polyubiquitination) in

MDA5^{K23R/K43R} and WT cells. These results indicate that the two lysine residues are specific for ISGylation, although it is possible that a temporal switch of these two PTMs at K43 can occur for fine-tuning the activation state of MDA5. Future studies are warranted to illustrate the dynamics and relative contributions of MDA5 PTMs in physiological (cell-based or in vivo) conditions using similar approaches as described herein for MDA5 CARD ISGylation.

Our identification of ISGylation as a physiologically important PTM governing MDA5-mediated immunity highlights its potential for translational applications. Recent studies have demonstrated that MDA5 plays a determining role in the immunogenicity of COVID-19 vaccines, particularly in stimulating humoral and cell-mediated adaptive immune responses (41). Although the involvement of specific PTMs in MDA5 activation by COVID-19 vaccines remains unknown, we postulate that ISGylation plays a role, and modulating MDA5 ISGylation may provide a strategy to enhance vaccine efficacy. Given that ISG15 conjugation to viral proteins typically inhibits their function, and further, since viruses such as SARS-CoV-2 have evolved tactics to actively remove ISGylation from both host and viral proteins (20, 25, 42), boosting ISGylation could offer dual benefits via 1) fortifying MDA5 (and perhaps other sensor such as cGAS) signaling, and 2) counteracting viral evasion through de-ISGylation. Along these lines, as sensing of endogenous host RNA ligands by MDA5 and *Mda5/Iffh1* gain-of-function mutations underlie certain autoimmune conditions (43–45), exploring the modulation of MDA5 ISGylation as an immunomodulatory approach to mitigate autoinflammation represents an intriguing area for future research. Overall, our findings unveiling a pivotal role of MDA5 CARD ISGylation in promoting innate immunity may hold promise for translational application in antiviral drug design, vaccinology, and autoimmunity.

Materials and Methods

Generation of MDA5^{K23R/K43R} and MDA5^{-/-} Mice. The *Mda5/Iffh1* transgenic mice were generated by introducing the K23R and K43R mutations into the native *Mda5/Iffh1* genomic DNA locus by replacing the WT exon1 with a double mutant exon1 directly in mice using CRISPR-Cas9 and a targeting vector. The sgRNA sequences that directed Cas9 nuclease cutting on either side of a *Mda5/Iffh1* exon1 genomic DNA target fragment were identified by the CRISPR algorithm (<http://crispor.tefor.net/>) and screened with a sgRNA in vitro screening system (Clontech). The cut sites for the 5' sgRNA *Mda5/Iffh1* 1162/rev (CATCGTGAGGTCTCAGGAAA) and the 3' sgRNA *Mda5/Iffh1* 1652/fw (CGGTAGGTGTCAATGTAGT) were then used to design a targeting vector containing a 1 kb 5' arm of homology, a unique *Ascl* site at the cut site of 1162/rev, a double mutant *Mda5/Iffh1* exon1 sequence, a unique *PmeI* site at the cut site of 1652/fw, and a 1 kb 3' arm of homology. The insertion of the unique sites prevents cutting the targeting vector by Cas9 nuclease. Mixtures of Cas9 nuclease, both sgRNAs, and the supercoiled targeting vector were microinjected into the pronucleus of fertilized oocytes from C57BL/6J mice at the Case Transgenic and Targeting Facility (Case Western Reserve University). Injected fertilized oocytes were transferred to the oviducts of CD1 pseudopregnant recipients and the resulting pups were transferred to the Gack laboratory. In genome editing, because of the two sgRNAs in the mixtures, the DNA repair machinery can also resolve the cuts by consecutive nonhomologous end joining, leading to the deletion of the intertwining WT *Mda5/Iffh1* exon1 sequence and resulting in a putative null allele. Animals were therefore screened for both knock-in (KI) and knock-out (KO) genotypes, with the latter serving as the matched control. MDA5^{K23R/K43R} and MDA5^{-/-} founder mice were then backcrossed to C57BL/6J WT mice (Jackson Laboratory) to generate homozygous MDA5^{K23R/K43R} and MDA5^{-/-} mice in the C57BL/6J background. Validation of the transgenic mice as well as additional information about the mouse lines used in this study are described in *SI Appendix, Methods*.

Mouse Infection Studies. For EMCV infection, sex-matched 6 to 8-wk-old WT, MDA5^{K23R/K43R}, and MDA5^{-/-} C57BL/6J mice were infected with the indicated plaque forming unit (PFU) of EMCV in 100 μ L of sterile PBS via the intraperitoneal

route following published protocols (34). Both female and male mice were used in the experiments. Mice were monitored daily for disease progression, and specific tissues were analyzed as described in detail in *SI Appendix, Methods*. All experiments were performed under protocols approved by the Institutional Animal Care and Use Committee of the Cleveland Clinic Florida Research and Innovation Center.

Cardiac Histology and Quantification of Myofiber-Free Space. Histological staining of cardiac tissues from uninfected or EMCV-infected WT, MDA5^{K23R/K43R}, and MDA5^{-/-} mice was performed as previously described with minor modifications (34) (see also *SI Appendix, Methods*).

The extracellular space between cardiac myofibers was quantified using ImageJ similarly as described previously (34). In brief, H&E-stained images (10 fields per mouse genotype; N = 5 mice per genotype) at 20 \times magnification were first converted to 8-bit grayscale images. Binary images were generated, and 3 to 6 regions of interest (ROIs) per field were selected ensuring a wide representative tissue sampling. The percentage of extracellular space within each ROI was quantified, and the average percentage of myofiber-free space was calculated for each mouse group. The total number of ROIs per treatment group was 50.

Cell Culture. MDFs derived from ear/tail tissue of WT, MDA5^{K23R/K43R}, and MDA5^{-/-} mice (C57BL/6J mice, 6 to 8-wk-old) were isolated after mincing and treatment with digestion media containing collagenase D (20 mg/mL) and pronase (20 mg/mL) (46). Cells were cultured in Roswell Park Memorial Institute (RPMI) media supplemented with 10% (v/v) FBS, 2 mM L-glutamine, 1 mM sodium pyruvate, 50 μ M 2-mercaptoethanol, and 100 U/mL antibiotic-antimycotic (Gibco). Bone marrow-derived macrophages (BMDMs) were generated from the femur and tibia of WT, MDA5^{K23R/K43R}, and MDA5^{-/-} mice (C57BL/6J background, 6 to 8-wk old) and maintained in RPMI media supplemented with 10% (v/v) FBS, 100 U/mL antibiotic-antimycotic (Gibco), 1% (v/v) nonessential amino acids (NEAA), 1 mM sodium pyruvate, and 25 μ g/mL macrophage colony-stimulating factor (M-CSF; Thermo Fisher Scientific) as previously described (16). The other cell lines used in this study are described in *SI Appendix, Methods*. All cell cultures were maintained at 37 $^{\circ}$ C in a humidified 5% CO₂ atmosphere. Primary cells from WT, MDA5^{K23R/K43R}, and MDA5^{-/-} mice were validated by genotyping. Additionally, the presence or absence of MDA5 protein expression was confirmed by immunoblot (IB) analysis. All cell lines have been regularly tested for the absence of *Mycoplasma* contamination by PCR assay and/or using the MycoAlert Kit (LT37-701; Lonza).

Viral RNA Isolation and Transfection. EMCV RNA was produced as previously described (20). Briefly, Vero cells were infected with EMCV (MOI 2) for 10 h, and total RNA was isolated using TRIzol Reagent (15596018, Thermo Fisher Scientific) per the manufacturer's instructions. Mock RNA and SARS-CoV-2 RNA were generated by isolating total RNA from Vero E6-TMPRSS2 cells that either remained uninfected or that were infected for 24 h with recombinant SARS-CoV-2 (strain K49; MOI 1) as detailed in previous publications (20, 47). EMCV RNA and SARS-CoV-2 RNA transfections were performed at the indicated concentrations using the Lipofectamine 2000 transfection reagent (11668019; Thermo Fisher Scientific). RABV_e was generated by in vitro transcription using the MEGAscript T7 Transcription Kit (Invitrogen) according to a previous protocol (24), and for its transfection into cells, Lipofectamine RNAiMAX Transfection Reagent (13778150; Invitrogen) was used (see respective Figure legends for details on RABV_e concentrations used).

Immunoprecipitation Assay and Immunoblot Analysis. Immunoprecipitation of endogenous proteins (i.e., MDA5 and SUMO1) was performed using standard protocols with minor modifications (13, 20). Briefly, for assaying endogenous MDA5 ISGylation and SUMOylation in MDF cells from WT and MDA5^{K23R/K43R} mice or in primary NHLFs, cells were stimulated as indicated and then lysed using Nonidet P-40 (NP-40) buffer [50 mM HEPES (pH 7.2 to 7.5), 200 mM NaCl, 1% (v/v) NP-40, 5 mM EDTA, and 1 \times protease inhibitor (Sigma)], followed by centrifugation at 16,000 \times g and 4 $^{\circ}$ C for 20 min. Centrifuged cell lysates were then precleared at 4 $^{\circ}$ C for 1 to 2 h using Protein G Dynabeads pre-conjugated with rabbit IgG (DA1E; CST). Next, cell lysates were incubated for 16 h with Protein G Dynabeads pre-conjugated with anti-MDA5 antibody (D74E4; CST) (in case of ISGylation) or anti-SUMO1 antibody (C9H1; CST) (in case of SUMOylation), or IgG isotype control (DA1E; CST), at 4 $^{\circ}$ C. The beads were extensively washed five times with NP-40 buffer. The proteins were eluted by heating in 1 \times Laemmli SDS sample buffer at

95 °C for 5 min. Protein samples were resolved on Bis-Tris SDS-polyacrylamide gel electrophoresis (PAGE) gels and transferred onto polyvinylidene difluoride (PVDF) membranes (1620177; Bio-Rad). Membranes were incubated with primary and secondary antibodies (at dilutions described in *SI Appendix, Methods*), and protein signals were visualized using an ImageQuant LAS 4000 Chemiluminescent Image Analyzer (General Electric) as previously described (20).

For determining the K63-linked ubiquitination of endogenous MDA5, cell lysates were prepared in a modified RIPA buffer [50 mM Tris-HCl (pH 7.5), 150 mM NaCl, 1% (v/v) NP-40, 2% (w/v) SDS, 0.25% sodium deoxycholate, and 1 mM EDTA] followed by boiling at 95 °C for 10 min, and sonication. The lysates were then diluted 10-fold with a modified RIPA buffer containing no SDS (final concentration of SDS at 0.2%) and then cleared by centrifugation at 20,000 × g for 20 min at 4 °C. The lysates were precleared as described above and then subjected to IP with anti-MDA5 (D74E4; CST) or IgG (isotype control), following published procedures (20).

Semidenaturing Detergent Agarose Gel Electrophoresis. Endogenous MDA5 oligomerization in EMCV RNA-stimulated MDFs isolated from WT and MDA5^{K23R/K43R} mice was determined by semidenaturing detergent agarose gel electrophoresis (SDD-AGE) as previously described (20).

Sequence Alignments. Primary sequence alignment of the amino acid regions containing K23 and K43 in orthologous MDA5 proteins was performed using Clustal Omega (1. 2. 4).

1. M. Motwani, S. Pesiridis, K. A. Fitzgerald, DNA sensing by the cGAS-STING pathway in health and disease. *Nat. Rev. Genet.* **20**, 657–674 (2019).
2. T. H. Mogensen, Pathogen recognition and inflammatory signaling in innate immune defenses. *Clin. Microbiol. Rev.* **22**, 240–273 (2009).
3. G. Liu, M. U. Gack, Distinct and orchestrated functions of RNA Sensors in Innate Immunity. *Immunity* **53**, 26–42 (2020).
4. A. Iwasaki, R. Medzhitov, Control of adaptive immunity by the innate immune system. *Nat. Immunol.* **16**, 343–353 (2015).
5. J. Rehwinkel, M. U. Gack, RIG-I-like receptors: Their regulation and roles in RNA sensing. *Nat. Rev. Immunol.* **20**, 537–551 (2020).
6. L. Naesens, F. Haerynck, M. U. Gack, The RNA polymerase III-RIG-I axis in antiviral immunity and inflammation. *Trends Immunol.* **44**, 435–449 (2023).
7. Z. Ma, G. Ni, B. Damania, Innate sensing of DNA Virus genomes. *Annu. Rev. Virol.* **5**, 341–362 (2018).
8. H. M. Lazear, J. W. Schoggins, M. S. Diamond, Shared and Distinct Functions of Type I and Type III Interferons. *Immunity* **50**, 907–923 (2019).
9. M. Yoneyama, H. Kato, T. Fujita, Physiological functions of RIG-I-like receptors. *Immunity* **57**, 731–751 (2024).
10. P. Beltrao, P. Bork, N. J. Krogan, V. van Noort, Evolution and functional cross-talk of protein post-translational modifications. *Mol. Syst. Biol.* **9**, 714 (2013).
11. K. Chen, J. Liu, X. Cao, Regulation of type I interferon signaling in immunity and inflammation: A comprehensive review. *J. Autoimmun.* **83**, 1–11 (2017).
12. Z. Sun, H. Ren, Y. Liu, J. L. Teeling, J. Gu, Phosphorylation of RIG-I by casein kinase II inhibits its antiviral response. *J. Virol.* **85**, 1036–1047 (2011).
13. E. Wies *et al.*, Dephosphorylation of the RNA sensors RIG-I and MDA5 by the phosphatase PP1 is essential for innate immune signaling. *Immunity* **38**, 437–449 (2013).
14. N. P. Maharaj, E. Wies, A. Stoll, M. U. Gack, Conventional protein kinase C- α (PKC- α) and PKC- β negatively regulate RIG-I antiviral signal transduction. *J. Virol.* **86**, 1358–1371 (2012).
15. M. U. Gack, E. Nistal-Villan, K. S. Inn, A. Garcia-Sastre, J. U. Jung, Phosphorylation-mediated negative regulation of RIG-I antiviral activity. *J. Virol.* **84**, 3220–3229 (2010).
16. D. Acharya *et al.*, Actin cytoskeleton remodeling primes RIG-I-like receptor activation. *Cell* **185**, 3588–3602.e3521 (2022).
17. M. U. Gack *et al.*, TRIM25 RING-finger E3 ubiquitin ligase is essential for RIG-I-mediated antiviral activity. *Nature* **446**, 916–920 (2007).
18. H. Oshiumi *et al.*, The ubiquitin ligase Riplet is essential for RIG-I-dependent innate immune responses to RNA virus infection. *Cell Host Microbe* **8**, 496–509 (2010).
19. X. Lang *et al.*, TRIM65-catalyzed ubiquitination is essential for MDA5-mediated antiviral innate immunity. *J. Exp. Med.* **214**, 459–473 (2017).
20. G. Liu *et al.*, ISG15-dependent activation of the sensor MDA5 is antagonized by the SARS-CoV-2 papain-like protease to evade host innate immunity. *Nat. Microbiol.* **6**, 467–478 (2021).
21. L. Sarkar, G. Liu, M. U. Gack, ISG15: Its roles in SARS-CoV-2 and other viral infections. *Trends Microbiol.* **31**, 1262–1275 (2023).
22. L. Gitlin *et al.*, Essential role of mda-5 in type I IFN responses to polyriboinosinic:Polyribocytidylic acid and encephalomyocarditis picornavirus. *Proc. Natl. Acad. Sci. U.S.A.* **103**, 8459–8464 (2006).
23. M. M. Hu, C. Y. Liao, Q. Yang, X. Q. Xie, H. B. Shu, Innate immunity to RNA virus is regulated by temporal and reversible sumoylation of RIG-I and MDA5. *J. Exp. Med.* **214**, 973–989 (2017).
24. J. J. Chiang *et al.*, Viral unmasking of cellular 5S rRNA pseudogene transcripts induces RIG-I-mediated immunity. *Nat. Immunol.* **19**, 53–62 (2018).

Quantification and Statistical Analysis. All data were analyzed using GraphPad Prism software (version 10). A two-tailed, unpaired Student's *t* test was used to compare differences between the two experimental groups in all cases. For statistical evaluation of mice survival, the log-rank (Mantel-Cox) test was performed. For the clinical score analysis, two-way ANOVA was used followed by Bonferroni's posttest. Significant differences are denoted by **P* < 0.05, ***P* < 0.01, ****P* < 0.001, and *****P* < 0.0001. Prespecified effect sizes were not assumed, and the number of independent biological replicates (N) is indicated for each dataset.

Data, Materials, and Software Availability. All study data are included in the article and/or *SI Appendix*.

ACKNOWLEDGMENTS. We thank David LePage and Ron Conlon at the Case Transgenic and Targeting Facility of Case Western Reserve University for their support in generating the MDA5 knock-in and control mice. We are grateful to Judith Drazba, John Peterson, Bridget Besse, and Apryl Helmick (all Cleveland Clinic Lerner Research Institute Imaging Core) and Ruofan Cao (Cleveland Clinic FRIC Imaging Core) for their assistance with the histology analysis. We also thank Shanti Ross (Cleveland Clinic FRIC) for assistance with mouse colony maintenance. This work was supported by NIH grant R37 AI087846 (to M.U.G.).

Author affiliations: *Florida Research and Innovation Center, Cleveland Clinic, Port St. Lucie, FL 34987

25. D. Shin *et al.*, Papain-like protease regulates SARS-CoV-2 viral spread and innate immunity. *Nature* **587**, 657–662 (2020).
26. J. S. Errett, M. S. Suthar, A. McMillan, M. S. Diamond, M. Gale Jr., The essential, nonredundant roles of RIG-I and MDA5 in detecting and controlling West Nile virus infection. *J. Virol.* **87**, 11416–11425 (2013).
27. H. Kato *et al.*, Differential roles of MDA5 and RIG-I helicases in the recognition of RNA viruses. *Nature* **441**, 101–105 (2006).
28. G. Liu, M. U. Gack, Insights into pandemic respiratory viruses: Manipulation of the antiviral interferon response by SARS-CoV-2 and influenza A virus. *Curr. Opin. Immunol.* **78**, 102252 (2022).
29. A. Dastur, S. Beaudenon, M. Kelley, R. M. Krug, J. M. Huijbregtse, Herc5, an interferon-induced HECT E3 enzyme, is required for conjugation of ISG15 in human cells. *J. Biol. Chem.* **281**, 4334–4338 (2006).
30. F. Okumura, W. Zou, D. E. Zhang, ISG15 modification of the eIF4E cognate 4EHP enhances cap structure-binding activity of 4EHP. *Genes Dev.* **21**, 255–260 (2007).
31. W. Zou, D. E. Zhang, The interferon-inducible ubiquitin-protein isopeptide ligase (E3) EFP also functions as an ISG15 E3 ligase. *J. Biol. Chem.* **281**, 3989–3994 (2006).
32. D. Oudshoorn *et al.*, HERC6 is the main E3 ligase for global ISG15 conjugation in mouse cells. *PLoS One* **7**, e29870 (2012).
33. L. Ketscher, A. Basters, M. Prinz, K. P. Knobloch, mHERC6 is the essential ISG15 E3 ligase in the murine system. *Biochem. Biophys. Res. Commun.* **417**, 135–140 (2012).
34. L. E. Bazzone *et al.*, ADAM9 promotes type I interferon-mediated innate immunity during encephalomyocarditis virus infection. *Nat. Commun.* **15**, 4153 (2024).
35. T. C. Xiong *et al.*, The E3 ubiquitin ligase ARIH1 promotes antiviral immunity and autoimmunity by inducing mono-ISGylation and oligomerization of cGAS. *Nat. Commun.* **13**, 5973 (2022).
36. C. Lin *et al.*, Regulation of STING activity in DNA sensing by ISG15 modification. *Cell Rep.* **42**, 113277 (2023).
37. Y. Qin *et al.*, ISGylation by HERCs facilitates STING activation. *Cell Rep.* **43**, 114135 (2024).
38. L. Chu *et al.*, HERC5-catalyzed ISGylation potentiates cGAS-mediated innate immunity. *Cell Rep.* **43**, 113870 (2024).
39. M. J. Kim, S. Y. Hwang, T. Imaizumi, J. Y. Yoo, Negative feedback regulation of RIG-I-mediated antiviral signaling by interferon-induced ISG15 conjugation. *J. Virol.* **82**, 1474–1483 (2008).
40. Y. Du *et al.*, LRR25 inhibits type I IFN signaling by targeting ISG15-associated RIG-I for autophagic degradation. *EMBO J.* **37**, 351–366 (2018).
41. C. Li *et al.*, Mechanisms of innate and adaptive immunity to the Pfizer-BioNTech BNT162b2 vaccine. *Nat. Immunol.* **23**, 543–555 (2022).
42. J. Zhu *et al.*, ISGylation of the SARS-CoV-2 N protein by HERC5 impedes N oligomerization and thereby viral RNA synthesis. *J. Virol.* **98**, e0086924 (2024), 10.1128/jvi.00869-24.
43. G. I. Rice *et al.*, Gain-of-function mutations in IFIH1 cause a spectrum of human disease phenotypes associated with upregulated type I interferon signaling. *Nat. Genet.* **46**, 503–509 (2014).
44. M. Funabiki *et al.*, Autoimmune disorders associated with gain of function of the intracellular sensor MDA5. *Immunity* **40**, 199–212 (2014).
45. J. A. Gorman *et al.*, The A946T variant of the RNA sensor IFIH1 mediates an interferon program that limits viral infection but increases the risk for autoimmunity. *Nat. Immunol.* **18**, 744–752 (2017).
46. M. Khan, S. Gasser, Generating primary fibroblast cultures from mouse ear and tail tissues. *J. Vis. Exp.* **107**, 53565 (2016), 10.3791/53565.
47. D. Cheng, J. Zhu, G. Liu, M. U. Gack, D. A. MacDuff, HOIL1 mediates MDA5 activation through ubiquitination of LGP2. *bioRxiv* [Preprint] (2024). <https://doi.org/10.1101/2024.04.02.587772> (Accessed 3 April 2024).